



**HAL**  
open science

# Solid-State and Solution Self-assembly Properties of Mono- and Bis-acetylide Ru-II Complexes Bearing Hydrogen-Bonding Amide Functions

Olivier Galangau, Elsa Caytan, William T. Gallonde, Isabelle de Waele, Franck Camerel, Stephane Rigaut

► **To cite this version:**

Olivier Galangau, Elsa Caytan, William T. Gallonde, Isabelle de Waele, Franck Camerel, et al.. Solid-State and Solution Self-assembly Properties of Mono- and Bis-acetylide Ru-II Complexes Bearing Hydrogen-Bonding Amide Functions. *European Journal of Inorganic Chemistry*, 2023, 26 (1), 10.1002/ejic.202200579 . hal-03884965

**HAL Id: hal-03884965**

**<https://hal.science/hal-03884965v1>**

Submitted on 5 Dec 2022

**HAL** is a multi-disciplinary open access archive for the deposit and dissemination of scientific research documents, whether they are published or not. The documents may come from teaching and research institutions in France or abroad, or from public or private research centers.

L'archive ouverte pluridisciplinaire **HAL**, est destinée au dépôt et à la diffusion de documents scientifiques de niveau recherche, publiés ou non, émanant des établissements d'enseignement et de recherche français ou étrangers, des laboratoires publics ou privés.

# What if your Chemistry research received 2x the citations and 3x the amount of downloads?



The benefits for you as an author publishing open access are clear: Articles published open access have wider readership and are cited more often than comparable subscription-based articles.

**Submit your paper today.**



# Solid-State and Solution Self-assembly Properties of Mono- and Bis-acetylide Ru<sup>II</sup> Complexes Bearing Hydrogen-Bonding Amide Functions

Olivier Galangau,<sup>\*,[a]</sup> Elsa Caytan,<sup>[a]</sup> William T. Gallonde,<sup>[a]</sup> Isabelle de Waele,<sup>[b]</sup> Franck Camerel,<sup>\*,[a]</sup> and Stéphane Rigaut<sup>\*,[a]</sup>

In this work, we report our latest results regarding the self-assembly properties of two Ru-acetylides complexes and their corresponding free organic ligands, in solution and in the solid state. The four compounds show mesogenic properties, which we have rationalized thanks to extensive DSC, SAXS, POM, FTIR and molecular dynamic investigations. We clearly establish that hydrogen bonds stabilize the supramolecular structures, and

that introducing the metal center and its coordination sphere induces large change in the liquid crystal properties. In addition, for the monoacetylide compound **Ru<sub>2</sub>**, solution-state studies helped us rationalize its supramolecular abilities. In particular, we demonstrate that **Ru<sub>2</sub>** follows an isodesmic growth supramolecular polymerization in aromatic solvent.

## Introduction

Since the discovery of the first mesogen more than a century ago, mesogens and metallomesogens are the subject of exciting research activities, particularly for display technologies.<sup>[1]</sup> Mesogens are anisotropic molecules that can promote the formation of a fluid and ordered liquid crystalline state. Thermotropic liquid crystals are obtained directly in solid state with molecules usually carrying several long carbon chains, in a specific temperature range. Lyotropic liquid crystals are obtained in a given solvent and the self-organization of the mesogen depends on its concentration and also on the temperature. Metallomesogens are defined as coordination or organometallic metal complexes endowed with mesomorphic, i.e. liquid crystalline, properties, and have known an increasing popularity in this continuously expanding field.<sup>[1c,d,2]</sup> Indeed, new resulting physical characteristics have emerged such as, geometries diverging from the standard mesogens, optoelectronic properties, magnetic properties or charge transport

abilities due to synergetic interactions between the metal and its ligands.<sup>[2,3,4]</sup> Rod-shaped (calamitic) and disc-shaped (discotic) derivatives are the most commonly encountered forms of metallomesogens. Among the calamitic compounds, metal-acetylides where the metal is Pt<sup>II</sup>, Au<sup>I</sup>, Au<sup>III</sup>, Rh<sup>III</sup>, Hg<sup>II</sup> were already reported and usually yield smectic or nematic mesophases.<sup>[2,5]</sup> Examples of Pt<sup>II</sup> or Au<sup>III</sup> acetylides were particularly detailed due to their attractive solid-state luminescence properties, which arises from strong metallophilic interactions (Pt–Pt or Au–Au).<sup>[6,7]</sup> Surprisingly, to the best of our knowledge metallomesogens of Ru<sup>II</sup> acetylides were not reported so far, yet they hold great promises in charge transport applications because of their low oxidation potentials,<sup>[8,9]</sup> probably because it was believed until recently that these species were too bulky to self-assemble. Recently, our group published a first example of calamitic-like Ru<sup>II</sup> bis-acetylides derivative (compound **Ru<sub>1</sub>**) that self-assembles into aromatic solvent thanks to hydrogen bonding interactions.<sup>[9]</sup> The compound forms micrometer long ribbons that eventually leads to the formation of a gel. As seen on Scheme 1, our

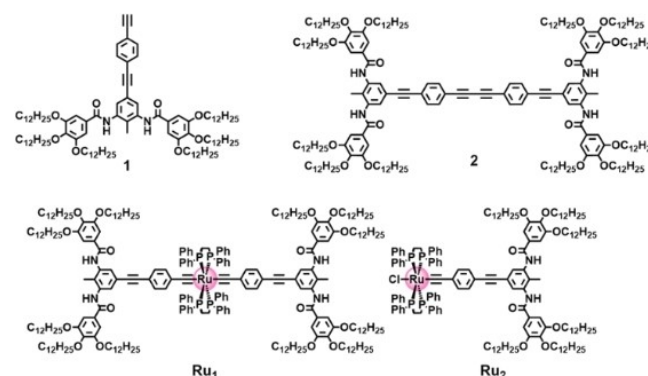
[a] Dr. O. Galangau, Dr. E. Caytan, W. T. Gallonde, Dr. F. Camerel, Prof. S. Rigaut  
Univ Rennes, CNRS, ISCR (Institut des Sciences Chimiques de Rennes) – UMR 6226,  
35000 Rennes, France  
E-mail: olivier.galangau@univ-rennes1.fr  
franck.camerel@univ-rennes1.fr  
stephane.rigaut@univ-rennes1.fr

[b] Dr. I. de Waele  
LASIRE, UMR 8516, Université des Sciences et Technologies de Lille  
59655 Villeneuve d'Ascq, France

Supporting information for this article is available on the WWW under  
https://doi.org/10.1002/ejic.202200579

Part of the "EurJIC Talents" Special Collection.

© 2022 The Authors. European Journal of Inorganic Chemistry published by Wiley-VCH GmbH. This is an open access article under the terms of the Creative Commons Attribution Non-Commercial License, which permits use, distribution and reproduction in any medium, provided the original work is properly cited and is not used for commercial purposes.



Scheme 1. Structures of the four derivatives under investigation.

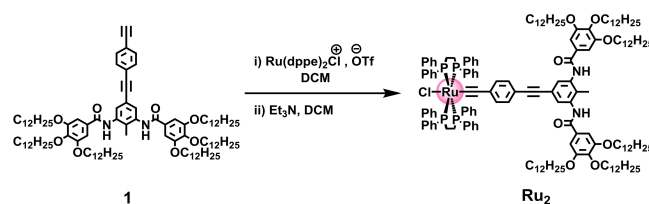
previous design encompasses a discotic functional alkynyl platform originally developed by one of us to design Pt<sup>II</sup> metallomesogens and possesses an inherent calamitic (rod-like) structure.<sup>[6]</sup> This observation prompted us to investigate the solid-state self-assembly abilities of our previous **Ru<sub>1</sub>** complex. Furthermore, to decipher the importance of each molecular fragment into the supramolecular packing, we designed and investigated the properties of a second monoacetylide complex where one chloride ligand remains, namely **Ru<sub>2</sub>**. Eventually, we have compared the organometallic compounds to their purely organic counterparts, *i.e.* the free alkynyl ligand **1** and the dimerized ligand, namely derivative **2**.

## Results and Discussion

**Synthesis.** Synthetic methodologies for compounds **1**, **2** and **Ru<sub>1</sub>** were previously reported.<sup>[9]</sup> Chloro-compound **Ru<sub>2</sub>** was prepared as shown in Scheme 2. The starting pro-ligand **1** was first converted into the corresponding vinylidene intermediate which was not isolated. Deprotonation by a weak organic base such as Et<sub>3</sub>N yields the corresponding *chloro*-Ru<sup>II</sup> monoacetylide complex in 74% yield. This compound was fully characterized by <sup>1</sup>H, <sup>13</sup>C, <sup>31</sup>P{<sup>1</sup>H}-NMR, HR-MS and FT-IR techniques. In particular, the presence of a singlet signal in the <sup>31</sup>P{<sup>1</sup>H}-NMR spectrum located at δ = 49 ppm confirms the *trans* configuration and the presence of a single acetylide ligand (Figure S1–S3).<sup>[10]</sup> This is also evidenced by the presence of two sets of signals for the aromatic protons located on the *dpepe* ancillary ligands.

Electrochemical data of **Ru<sub>2</sub>** derivative were recorded in DCM with TBAPF<sub>6</sub> as supporting electrolyte at a scan rate of 0.1 V/s (see Figure S4). Compound **Ru<sub>2</sub>** features a reversible one-electron oxidation process located at 0.43 V vs SCE (see Table S1). The photophysical properties of **Ru<sub>2</sub>** were also investigated in DCM (Figure S5). The complex displays an intense absorption band located at 400 nm assigned to a d/π-π\* transition, based on our (TD)DFT calculations (see supporting information Figures S6–S7, Tables S2–S3). Altogether, these results are classically observed for monoacetylide complexes.<sup>[10]</sup>

**Mesogen properties.** The thermotropic properties of compounds **1**, **2**, **Ru<sub>1</sub>** and **Ru<sub>2</sub>** were investigated by a combination of polarized optical microscopy (POM), differential scanning



Scheme 2. Synthetic route to compound **Ru<sub>2</sub>**.

calorimetry (DSC) and small-angle X-ray diffraction (SA-XRD). The measured transition temperatures, enthalpy values and mesophase parameters are given in Table S4.

**Compound 1.** We have conducted DSC experiments concomitant with POM observations. Three perfectly reversible phase transitions centered at 59.65 °C, 74.5 °C and 157.0 °C were identified (Figure 1, top). At temperature higher than 180 °C, compound **1** underwent decomposition. Therefore, we could not reach an isotropic state. When the temperature was maintained below 180 °C, DSC traces were reversible. On

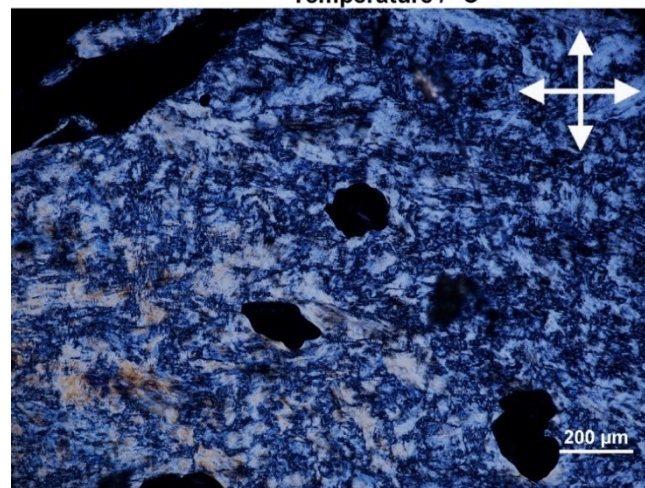
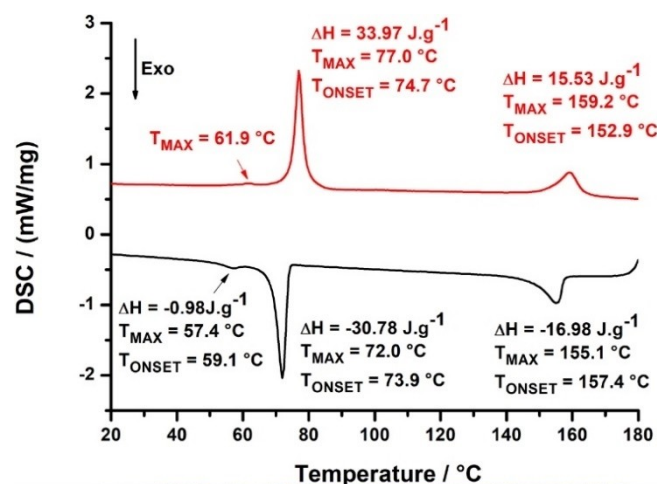


Figure 1. (Top) DSC trace of compound **1** (Top: 2<sup>nd</sup> heating curve; bottom: 1<sup>st</sup> cooling curve). (Bottom) compound **1** observed by optical microscopy between crossed-polarizers at 180 °C (crossed-polarizers symbolized by the white cross in the corner of the picture).



Olivier Galangau obtained his PhD in chemistry in 2011 from École Normale Supérieure de Cachan, under the supervision of Prof. P. Audebert. Following his postdoctoral training with Prof. T. Kawai at NAIST (Japan), he moved to Institut des Sciences Chimiques de Rennes (France) working with Dr. F. Pointillart. Since October 2018, he joined the group of Prof. S. Rigaut as CNRS research fellow. He is interested in developing new type of smart molecular/supramolecular materials, combining light- and/or electro-switchability for applications in organic (organometallic) electronics.

cooling, above 157 °C, compound **1** is in a birefringent fluid state as observed by POM, highlighting the formation of a liquid crystalline phase (Figure 1, bottom). Since the isotropic phase was not reached, no clear texture could be developed and, therefore, no correct assignment of phase symmetry can be made by POM. Fortunately, the SAXS patterns recorded at 170 °C display several sharp peaks in the small angle region, which was indexed in a 2D rectangular cell ( $a = 64.28 \text{ \AA}$ ,  $b = 21.90 \text{ \AA}$ ) with the  $C2mm$  space group (Figure 2, top). The SAXS patterns also display a broad halo centered at  $4.66 \text{ \AA}$  ( $h_{ch}$ ), characteristic of carbon chains in a molten state and confirms the fluid nature of this organized phase. An additional signal

( $h_0$ ) centered at  $4.2 \text{ \AA}$  is also observed in the wide-angle region and is attributed to the stacking distance between the ligand cores, as it was previously observed in the literature.<sup>[6]</sup>

These results point towards the formation of a rectangular columnar mesophase organization. In rectangular columnar mesophase ( $Col_r$ ), the columnar cross-section is not circular but more likely adopts an elliptical shape, and the particular arrangement of the elliptical columnar cross-sections leads to a rectangular lattice.<sup>[11]</sup> Such elliptical shape can be generated if two molecules are arranged into head-to-tail dimers. Several previously reported crystal structures have indeed shown that this organic platform has a strong tendency to stack head-to-tail in columns.<sup>[12]</sup>

These columns are usually stabilized by two strong 1D hydrogen bonding networks running in opposite direction along the stacking axis. To further confirm this assessment, we have performed FTIR measurements at 170 °C (see Figure S8). The spectrum features a N–H stretching vibration at  $3248 \text{ cm}^{-1}$  and a C=O stretching vibration at  $1648 \text{ cm}^{-1}$ . Both are characteristic of hydrogen bonding interaction. Moreover, the presence of one signal for the C=O bond vibration clearly indicates that all the molecules are self-assembled thanks to those hydrogen bonding interactions. Overall, at 170 °C, compound **1** forms head-to-tail stacks which further leads to columns and these columns are arranged into a rectangular lattice. The mutual organization of these columns into a rectangular lattice leads to the formation of the  $Col_r$  mesophase.

Molecular dynamics (MD) simulations (see supporting information) further supported the existence of a columnar organization of head-to-tail dimers at 170 °C with a rectangular lattice, where the fatty chains perfectly fill the space in between the columnar stack of aromatic cores (Figure S12). In particular, the simulation has indicated a molecular stacking distance of  $4.2 \text{ \AA}$ , in excellent agreement with the SAXS experimental data.

The SAXS patterns recorded between 157.0 °C and 74.5 °C all display series of sharp peaks in the small angle region which can be indexed in an oblique lattice ( $Col_o$  phase) (Figure 2, middle) with the following lattice parameters  $a = 40.40 \text{ \AA}$ ,  $b = 32.62 \text{ \AA}$  (Figure 2, bottom). An additional broad signal at  $4.5 \text{ \AA}$  ( $h_{ch}$ ) confirms the molten state of the alkyl chains and the persistence of a liquid crystalline state. As previously observed at higher temperature, the broad signal at  $4.2 \text{ \AA}$ , assigned to the stacking of the extended aromatic cores through hydrogen bonding, is also observed. This result suggests the head-to-tail stacking of molecules remains. The observed contraction is consistent with decreasing temperature and the emergence of the oblique phase is likely due to a reorientation of the elliptical axis of the columns at the transition. FTIR measurement performed at 100 °C features a single N–H stretching vibration at  $3185 \text{ cm}^{-1}$  and a single C=O stretching vibration at  $1638 \text{ cm}^{-1}$ . This firmly confirms that the molecules are tightly interacting through hydrogen bonding (Figure S9). Interestingly, from 170 °C to 100 °C the N–H vibration decreases from  $3236 \text{ cm}^{-1}$  to  $3185 \text{ cm}^{-1}$  ( $51 \text{ cm}^{-1}$ ) while the variation of the C=O vibration is negligible (see Table S5). This is indicative of the strengthening of the hydrogen bonding interaction when

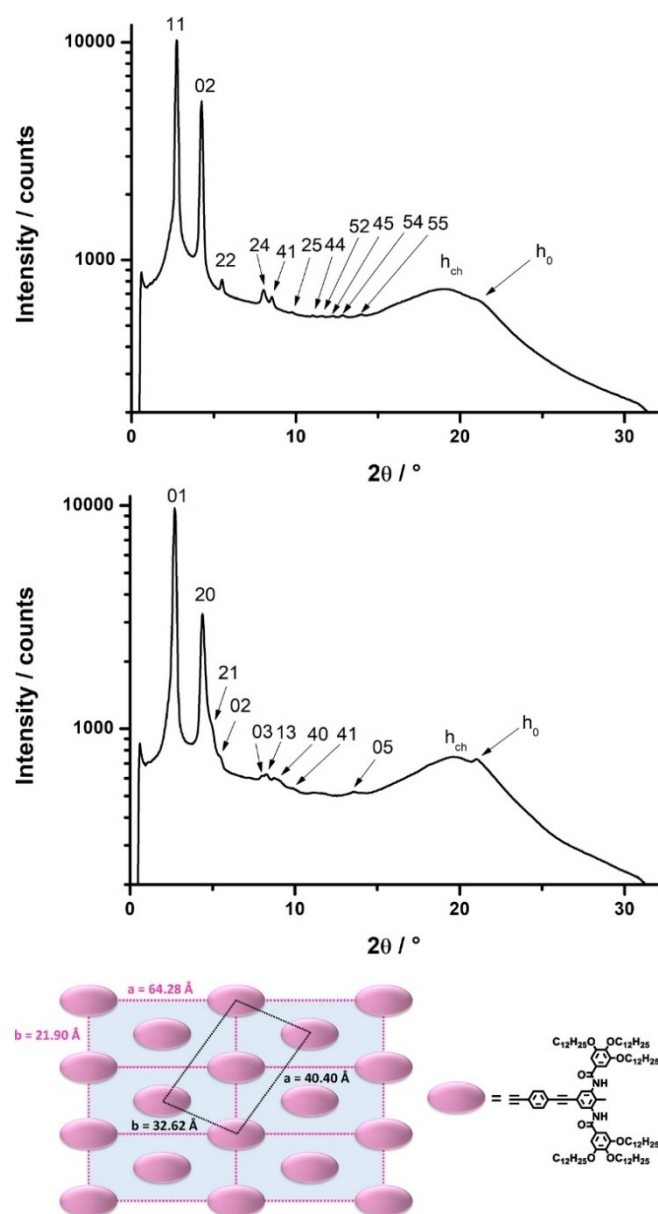


**Figure 2.** SAXS pattern after second heating of compound **1** at 170 °C (Top), at 100 °C (Middle) ( $h_k$  indexation,  $h_{ch}$ : maximum of the diffuse scattering due to lateral distances between molten aliphatic tails,  $h_0$ : diffuse scattering due to  $\pi$ - $\pi$  stacking. (Bottom) Schematics of the rectangular (pink) and oblique (black) unit cell found at 170 °C and 100 °C, respectively.

cooling down the sample and transiting from a Col<sub>r</sub> to a Col<sub>o</sub> arrangement.

This Col<sub>o</sub> mesophase was also simulated by MD at 157 °C and the modelling was in good agreement with the experimental data (Figure S13) exhibiting stable columnar organization. Upon further cooling, another phase transition was detected at 74.5 °C and is attributed to a mesophase to crystal phase transition, as revealed by the apparition of numerous sharp diffraction peaks on the SAXS patterns over the whole 2θ range explored. Finally, the small phase transition observed at low temperatures around 59 °C is attributed to a crystal to crystal phase transition. FTIR at 25 °C that features one N–H vibration at 3157 cm<sup>-1</sup> and one C=O vibration at 1637 cm<sup>-1</sup>.

These values are again symptomatic of molecules fully associated thanks to strong hydrogen bonding interactions. As observed previously, the N–H vibration experiences a further decrease of 28 cm<sup>-1</sup>, indicative of a strengthening of this supramolecular interaction. Altogether, compound **1** shows liquid crystallinity from 74 °C up to the decomposition at ca 180 °C and relies on a permanent and dense network of hydrogen bonding interactions on the investigated temperature range.

**Compound 2.** As seen on the DSC scan, **2** presents a single reversible thermal transition centered at 85 °C (Figure 3). Successive DSC scans revealed that compound **2** is not stable above 180–200 °C. Indeed, prolonged heating above these temperatures induces a marked decrease in intensity and a shift in DSC peaks. Above 85 °C, POM observations have shown that derivative **2** is in a soft and birefringent state. No texture could be properly developed since the isotropic state could not be reached. The SAXS patterns recorded at 150 °C display several sharp peaks in the small angle region, which can be properly indexed as reflections from a lattice of 2D rectangular ( $a = 22.43 \text{ \AA}$ ,  $b = 59.35 \text{ \AA}$ ) symmetry (Figure 3, bottom). The broad halo centered at 4.6 Å indicates that the carbon chains are in a molten state and confirms the formation of a liquid crystalline phase. As for compound **1**, a broad halo ( $h_0$  in Figure 3, bottom) is observed at 4.2 Å and is reminiscent of an intermolecular stacking through hydrogen bonds. Therefore, above 85 °C, **2** self-organizes into a Col<sub>r</sub> fashion, with a stacking distance of 4.2 Å.

FTIR measurements performed at 150 °C consistently confirm the existence of strong hydrogen bonds with N–H stretching vibration appearing at 3198 cm<sup>-1</sup> and C=O stretching vibration located at 1637 cm<sup>-1</sup> (Figure S9). Interestingly, standard geometrical treatment highlights that only one molecule is present in the rectangular unit cell  $h_0$ -thick as opposed to two molecules for compound **1**.

Such peculiar organization should originate from the elliptical shape of the molecular scaffold of **2**. To confirm that, molecular dynamic simulations have been performed with the parameters extracted at 150 °C (see Figure S14 supporting information). This MD modelling indicates that compound **2** forms columns made of molecules packing on top of each other, through hydrogen bonding interactions in parallel fashion. Interestingly, a stacking distance of 4.2 Å was also found, in excellent agreement with the SAXS data. As for

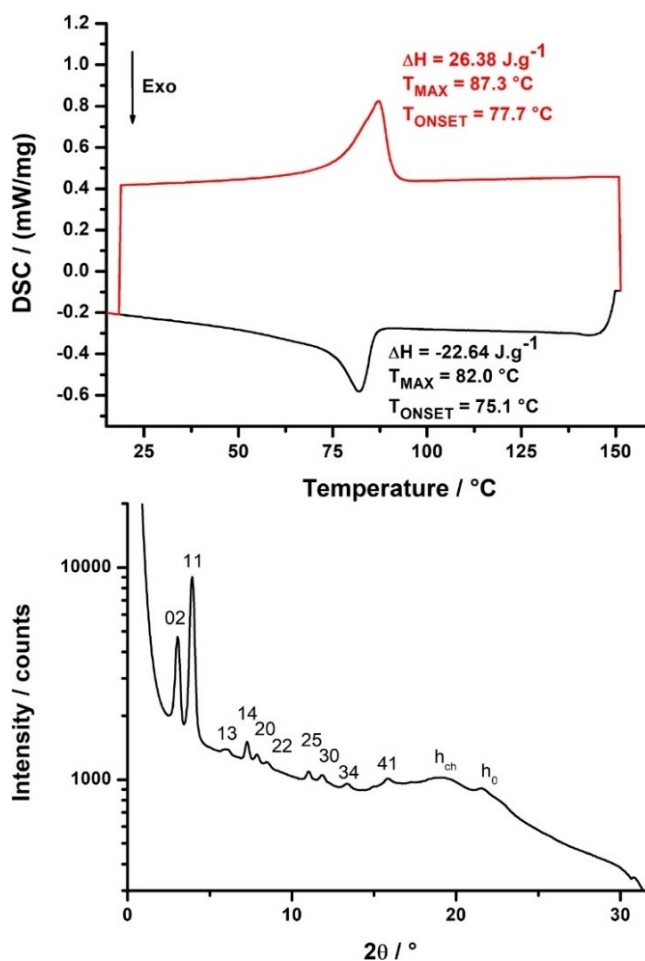


**Figure 3.** (Top) DSC trace of compound **2** (Top: 2<sup>nd</sup> heating curve; bottom: 1<sup>st</sup> cooling curve). (Bottom) SAXS pattern of compound **2** at 150 °C (second heating) with peak indexation.

compound **1**, the voids around the columnar stacks are filled with the long fatty chains.

On cooling, SAXS patterns recorded below 85 °C show a sharpening of the diffraction peaks in the wide-angle region typically associated with crystallization of the carbon chains and confirm that the phase transition observed on the DSC traces is due to a mesophase to crystal phase transition. Interestingly, FTIR measurements at 25 °C show a N–H vibration located at 3180 cm<sup>-1</sup> and a C=O vibration at 1637 cm<sup>-1</sup>. Remarkably, the N–H vibration experiences a slight shift from 3198 cm<sup>-1</sup> to 3180 cm<sup>-1</sup> at 150 °C and 25 °C, respectively. This means that the packing of **2** also relies on a strong and dense network of hydrogen bonds at all temperatures. Interestingly, the shift observed on cooling from 150 °C to 25 °C for **2** (18 cm<sup>-1</sup>) is less important than for **1** (59 cm<sup>-1</sup>), reflecting more robust intermolecular interactions in **2** than in **1**. Overall, dimerization of compound **1** into **2** goes not only with a drastic supramolecular packing change, from head-to-tail to face-to-face interactions, but also with an increase of the intermolecular interactions strength.

**Compound Ru<sub>1</sub>.** No thermal transition has been detected by DSC between  $-25^{\circ}\text{C}$  and  $200^{\circ}\text{C}$ . Yet, DSC analyses revealed that this compound strongly degrades after successive heating up to  $250^{\circ}\text{C}$ . In parallel, this degradation goes also with the observation of an isotropic state above  $250^{\circ}\text{C}$  as seen on POM. Anyway, since Ru<sub>1</sub> degrades after heating to  $250^{\circ}\text{C}$ , we decided to restrict our study to temperatures below  $200^{\circ}\text{C}$ . Below this limit, compound Ru<sub>1</sub> is a soft and malleable birefringent material as seen under POM (Figure 4, bottom), a good indication of its liquid crystalline nature. However, here again, no clear texture could be developed because no stable isotropic state could be reached.

SAXS patterns were recorded between  $30$  and  $180^{\circ}\text{C}$  upon heating and cooling. Analysis of these patterns has revealed that a broad phase transition occurs between  $30$  and  $80^{\circ}\text{C}$ , not detected by DSC. Above  $80^{\circ}\text{C}$ , all the SAXS patterns recorded up to  $180^{\circ}\text{C}$  are similar (Figure 4, top). They display series of sharp peaks in the small angle region together with a broad peak around  $20^{\circ}$  in  $2\theta$ , indicative of a liquid crystalline state. The small angle diffraction peak can be indexed in two distinct networks. A first set of diffraction peaks was indexed as the three first reflections of a lamellar phase and a second set of diffraction peaks was indexed in a 2D rectangular lattice. Therefore, we suggest that Ru<sub>1</sub> is organized into lamellae with the ruthenium centers arranged into a rectangular lattice within the lamellae. At  $180^{\circ}\text{C}$ , the lamellar periodicity is about  $27\text{ \AA}$  and the rectangular lattice parameters are  $a=20.27$  and  $b=14.62\text{ \AA}$ . The length of the molecule in its fully extended form is about  $65\text{ \AA}$ . This is indicative of a strong interdigitation of the complexes in the mesophase. The distance between the two organic platforms on the molecule was estimated to be about  $33\text{ \AA}$  and is close to the measured lamellar distance. Thus, the molecules are likely organized in lamellae, slightly tilted, with at least partial overlap of the organic fragments and the long carbon chains filling the space between the 1,2-dppe/ruthenium moieties organized in a rectangular array inside the lamella. Interestingly, this result echoes with the ability of Ru<sub>1</sub> to form gels in aromatic solvents.<sup>[9]</sup> Indeed, in our previous study, we investigated by SAXS and FTIR the compound supramolecular packing within the gel and found that Ru<sub>1</sub> self-organized into lamellae by means of hydrogen bonds and by segregating the aromatic cores from the aliphatic parts.

As expected, FTIR measurement on a pristine sample (Figure S10) at room temperature of compound Ru<sub>1</sub> has featured stretching vibrations of the amide function located at  $1635\text{ cm}^{-1}$  and a N–H stretching vibration at  $3244\text{ cm}^{-1}$ , confirming the lamellar organization is relying on a dense network of hydrogen bonding interactions. The fact that a single vibration band appears on the spectra is fully consistent with all amide functions of Ru<sub>1</sub> molecules being involved in the hydrogen bonds network.

Additional MD simulations (see supporting information) further support the experimental lamellar organization. In particular, the long aliphatic chains tend to embed the Ru-(dppe)<sub>2</sub> moieties leading to strong segregation between the aliphatic organic fragment and the aromatic ancillary ligands.

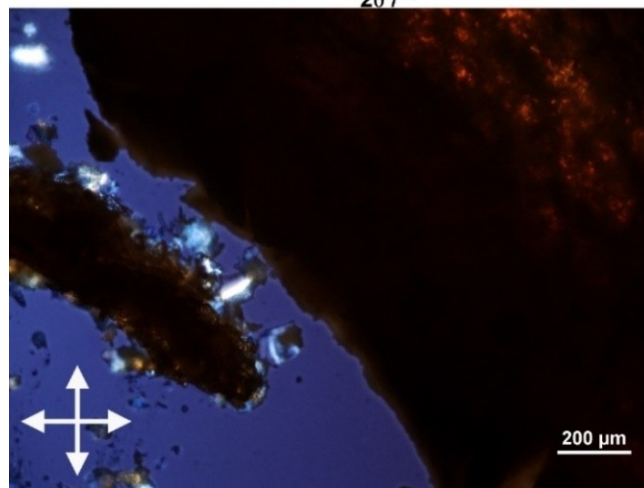
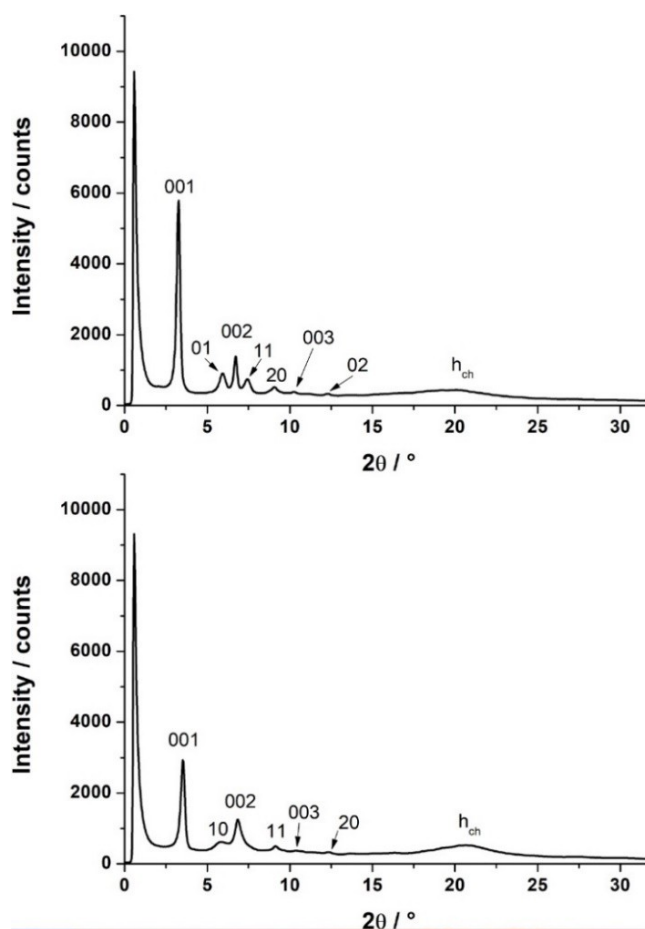


**Figure 4.** (Top) Indexed SAXS pattern recorded at  $180^{\circ}\text{C}$  for Ru<sub>1</sub>. (Middle) Indexed SAXS pattern recorded at  $30^{\circ}\text{C}$  for Ru<sub>1</sub>. (Bottom) POM image of Ru<sub>1</sub> at  $200^{\circ}\text{C}$  (crossed-polarizers symbolized by the white cross in the corner of the picture).

Upon further cooling, SAXS measurements indicate a gradual decrease in the peak intensities and a slight shift in the peak positions toward shorter distances. A transition, not detected by neither POM nor DSC, is clearly visible between  $80^{\circ}\text{C}$  and  $30^{\circ}\text{C}$  with the apparition of new sets of diffraction peaks (Figure 4, middle). Keeping the lamellar organization, at

30 °C, two sets of sharp diffraction peaks can be identified. The first set corresponds to the diffraction from the lamellar phase and the second can be tentatively indexed as the diffraction peaks coming from a 2D square lattice ( $a = 14.32 \text{ \AA}$ ). Thus, the broad phase transition detected between 30 °C and 80 °C is probably due to a reorganization of the ruthenium complexes inside the lamellas from a rectangular to a square organization. The broad halo, indicative of the molten state of the carbon, is still visible around 20°, meaning that the compound is still in a liquid crystalline state at room temperature. Interestingly, as opposed to **1** and **2**, SAXS patterns of **Ru<sub>1</sub>** do not feature any broad halo ( $h_0$ ) at around 4.2 Å. This suggests that the intermolecular arrangement does not involve a head-to-tail packing of the ligands, as already suggested by our previous Variable-Temperature NMR studies.<sup>[9]</sup> Overall, going from **2** to **Ru<sub>1</sub>**, it is clear that introducing a sterically demanding moiety such as the [Ru(dppe)<sub>2</sub>] induces a major change in the assembly, from columnar to lamellar and prevents a head-to-tail or a face-to-face packing of the organic ligands.

**Compound Ru<sub>2</sub>**. The DSC traces of compound **Ru<sub>2</sub>** display one single reversible transition centered at 194 °C (Figure 5, top left). Above 204 °C, the compound is in an isotropic state as revealed by POM observations (Figure 5a, bottom left). Upon slow cooling, a texture displaying pseudo-fan shaped texture, characteristic of columnar mesophases, readily develops below 188 °C (Figure 5b, bottom right).<sup>[13]</sup> Gentle pressure on the top cover-glass slide show that the material is soft and malleable, confirming the formation of a liquid crystalline phase. Below 188 °C, The SAXS patterns all display several sharp peaks in the small angle region which can tentatively be indexed as the reflections of a 2D rectangular lattice with parameters  $a = 73.55$  and  $b = 48.96 \text{ \AA}$ . The broad halo centered at 4.47 Å confirms that the compound is in a liquid crystalline state. As for derivative **Ru<sub>1</sub>**, the peak at around 4.2 Å reminiscent of the head-to-tail packing of the organic fragment was not detected.

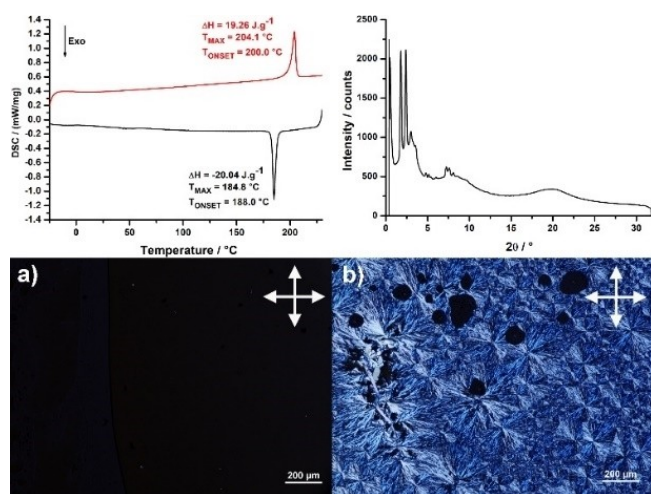


**Figure 5.** (Top left) DSC trace of **Ru<sub>2</sub>** (Top: 2nd heating curve; bottom: 1st cooling curve). (Top right) SAXS pattern of **Ru<sub>2</sub>** at 150 °C (second heating). (Bottom) a) POM image of **Ru<sub>2</sub>** at 180 °C and b) at 173 °C after cooling from the isotropic state (crossed-polarizers symbolized by the white cross in the corner of the picture).

This suggests that as for the symmetric complex, **Ru<sub>2</sub>** self-assembles in a different way compared to compounds **1** and **2**. Two underlying broad halos centered on 30 and 13 Å are also observed and can be attributed to the liquid-like order of large objects, i.e. a clustering of the Ruthenium/1,2-dppe fragments. The 30 Å dimension fits with the distance between two metallic centers assuming two molecules stacking in a head-to-tail fashion, while the 13 Å matches the metal coordination sphere diameter. This is in line with the solution state self-assembly behavior that we have observed as well (*vide infra*). Overall, derivative **Ru<sub>2</sub>** is in a liquid crystalline state from –20 °C up to the isotropization centered at 194 °C. Unfortunately, we were not able to determine neither the lattice space group nor the unit cell. Therefore, the exact packing of the complexes cannot be easily anticipated.

VT-FTIR measurements at 150 °C, 130 °C and 25 °C suggest that molecules of **Ru<sub>2</sub>** also self-organize thanks to hydrogen bonding interactions involving all amide functions (Table S5). From 150 °C down to 25 °C, the N–H stretching vibration band experiences a significant red-shift from 3226  $\text{cm}^{-1}$  to 3180  $\text{cm}^{-1}$ , consistent with a strengthening of the supramolecular interaction on cooling (Figure S11). As far as the C=O vibration is concerned, no shift was observed. In addition, as for **Ru<sub>1</sub>**, a single vibration band is observed whatever the temperature, which is consistent with all amide functions being involved in the hydrogen bonds network.

Note that, at 25 °C the N–H vibrations of **Ru<sub>1</sub>** appears at higher frequencies than for **Ru<sub>2</sub>**, indicative of a weaker supramolecular interaction for **Ru<sub>1</sub>** than for **Ru<sub>2</sub>**. At 25 °C, while the C=O band vibration is similar for all compounds, the N–H band vibrations vary drastically. The red-shift of this band vibration follows the following trend: compound **1** (3157  $\text{cm}^{-1}$ ), then **2** (3180  $\text{cm}^{-1}$ ) and **Ru<sub>2</sub>** (3180  $\text{cm}^{-1}$ ) and finally **Ru<sub>1</sub>** (3244  $\text{cm}^{-1}$ ).

This suggest that at 25 °C molecules of **1** are strongly interacting compare to molecules of **Ru<sub>1</sub>**.

Overall, compounds **1**, **2**, **Ru<sub>1</sub>** and **Ru<sub>2</sub>** feature thermotropic liquid crystal behavior, all relying on a dense network of hydrogen bonding interactions. Interestingly, all the solid-state data regarding compound **Ru<sub>1</sub>** are in good matching with its solution-state behavior (supramolecular polymerization leading to gel formation). In particular, our previous VT-NMR yielded precious information regarding its self-assembly.<sup>[9]</sup> The data clearly corroborate that **Ru<sub>1</sub>** self-assembled in solution thanks to hydrogen bonds with a packing that differs from head-to-tail. We thus anticipated that **Ru<sub>2</sub>** also self-organizes in aromatic solvent and we performed VT-NMR experiments in order to get more insight into the self-assembly of **Ru<sub>2</sub>**.

**Self-assembly of Ru<sub>2</sub> in solution.** Derivative **Ru<sub>2</sub>** is insoluble in alkane solvents but becomes soluble in aromatic solvents such as benzene or toluene. Interestingly, as opposed to **Ru<sub>1</sub>**, compound **Ru<sub>2</sub>** does not form any gel at room temperature. Rather, the compound is perfectly soluble up to a concentration of 107 mM. Thus, this clearly demonstrates the importance of the symmetric nature of the complex to obtain gelation properties. However, we took advantage of this difference to observe a proof of self-assembly on a wide range of temper-

ature and concentration. To do so, we first performed a dilution experiment of a solution in  $C_6D_6$  of  $Ru_2$ , from 4 mM down to 0.9 mM. This experiment evidenced remarkable signal shifts, which are reminiscent of some supramolecular interactions in the solution state (Figure S16). Most important is the upfield shift experienced by the amido protons from 7.65 ppm to 7.30 ppm, suggesting the involvement of some hydrogen bonding interactions for the construction of the supramolecular objects. Other signals also experience noticeable chemical shift changes over the dilution experiment. The singlet signal assigned to the methyl group on the central phenyl displays a slight upfield shift from 2.25 ppm to 2.0 ppm. Additionally, the singlet signal ascribed to the aromatic protons assigned to the toluyl fragment and located at 7.95 ppm at 4 mM experiences a downfield shift up to almost 8.0 ppm. This suggests these protons are in aromatic interaction at the highest concentration. As expected, the signals assigned to the *dpe* fragments do not show any change, underlying that these moieties are not involved in the supramolecular process. Therefore, these observations are consistent with those observed with  $Ru_1$  and show that  $Ru_2$  self-assembles in aromatic solvents and its assembly primarily involves some H-bonding but also to some extent partial CH- $\pi$  or/and  $\pi$ - $\pi$  stacking interactions.

In addition, we performed complementary VT-NMR experiments to disclose the supramolecular mechanism at stake. A solution in toluene- $d_8$  with a concentration of 10 mM was then studied by  $^1H$  NMR between 273 K and 360 K, with a cooling rate of 0.5 K/min and an equilibration time of 8 mins for each measurements.<sup>[14]</sup> The results are presented in Figure 6 and in Figure S17. At the lowest temperature, the amido proton signal

broadens and resonates at approximately 8.8 ppm. This suggests multiple hydrogen bonding interactions where the proton is in exchange. Warming the sample induces the largest upfield shift down to 7.35 ppm, suggesting a strong weakening of the hydrogen bonding interaction at high temperature. The methyl singlet signal also experiences an upfield shift as the temperature increases. Finally, the aromatic signal located at 7.8 ppm (aromatic protons located on the toluyl fragment) at 273 K experiences a downfield shift to reach almost 8 ppm at 360 K. These observations are identical to what we observed for  $Ru_1$  in our previous VT-NMR studies,<sup>[9]</sup> suggesting that  $Ru_2$  self-assembles in a similar way, and are in line with the dilution experiment mentioned earlier and clearly testify of a supramolecular ability.

The plotting of the chemical shift variation of the latter signal as a function of temperature features a clear plateau at  $\sim 350$  K (Figure 6). This profile was fitted with an isodesmic model,<sup>[14]</sup> which gave an excellent agreement (Figure 6 and S18). Isodesmic growth relies on a single association constant for successive assemblies on the stacks. As opposed to the well-known cooperative mechanism,<sup>[15]</sup> there is no critical concentration and/or temperature above which the supramolecular assembly can proceed. We found a melting temperature,  $T_m$ , defined as the temperature at which 50% of the aggregates are remaining in the solution of 303.5 K. The fitting also afforded a  $\Delta H_0 = -65 \text{ kJ mol}^{-1}$ ,  $\Delta S_0 = -166 \text{ J K}^{-1} \text{ mol}^{-1}$  meaning the supramolecular assembly seems to be enthalpically driven. The dimensionless equilibrium constant of polymerization at 290 K was found to be approximately  $100 \text{ M}^{-1}$ . Such a small value illustrates the weak self-association of  $Ru_2$  and explains why this

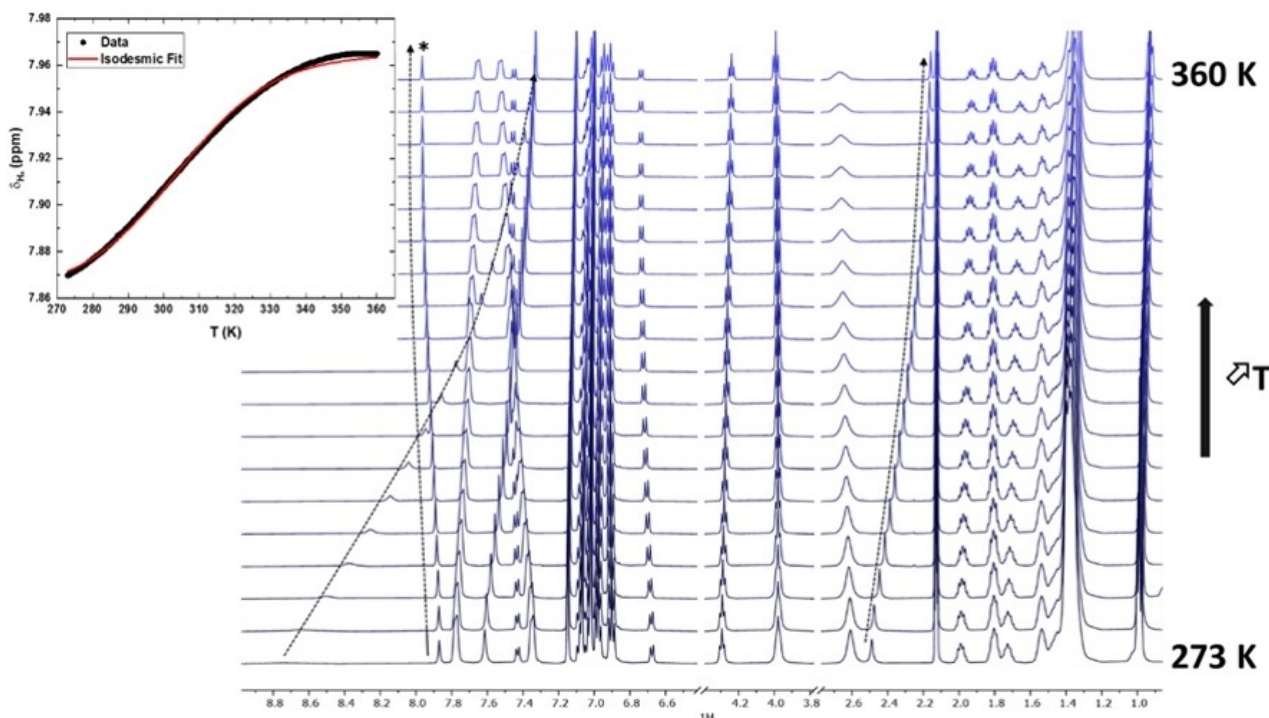


**Figure 6.** VT- $^1H$  NMR monitoring of a 10 mM solution of  $Ru_2$  in toluene- $d_8$ . (Inset) Plotting of the chemical shift variation of the singlet signal marked with a (\*) as a function of the temperature.

molecule is unable to form supramolecular polymers that would eventually lead to gel formation, like for **Ru**<sub>1</sub>. Indeed, at such temperature, **Ru**<sub>2</sub> barely forms dimers (the average number degree of polymerization is close to 2).

Overall, dilution and VT-NMR experiments have clearly evidenced that **Ru**<sub>2</sub> self-assembles in aromatic solvents like **Ru**<sub>1</sub> does, yet with not gelation and a poor efficiency probably due to the presence of a major sterically demanding [Ru(dppe)<sub>2</sub>Cl] fragment and less interaction with only one ligand. Further evidence of self-assembly at 10 mM concentration in toluene-d<sub>8</sub> could be obtained by performing a 2D NOESY <sup>1</sup>H-<sup>1</sup>H NMR experiment, at 273 K with a mixing time of 150 ms to avoid contamination by spin diffusion (Figure S19). A dipolar correlation was found between aromatic protons, doublet signal located at 7.43 ppm and the methyl signal at 2.48 ppm. Such a correlation can only be rationalized on the bases of a supramolecular interaction, the two protons being distant of 9 Å according to our DFT-optimized molecular geometry (see supporting information).

Finally, the central role of the hydrogen bonds was also highlighted by some FTIR measurements at room temperature of the same solution (Figure S20). Interestingly, the spectrum features two different vibrations at 1682 cm<sup>-1</sup> and 1657 cm<sup>-1</sup> assigned to free and H-bonded C=O stretching vibrations, respectively. This suggests that **Ru**<sub>2</sub> self-assembles in solution thanks to hydrogen bonding interactions as shown by VT-NMR and in a similar manner to **Ru**<sub>1</sub>. However, the presence of a free from H-bonds stretching vibration supports the fact that as opposed to **Ru**<sub>1</sub>, **Ru**<sub>2</sub> forms small aggregates (dimers) at room temperature and therefore goes in line with a poor self-assembly ability associated with a small association constant.

Combining those data, we finally propose a model packing (Figure S19) where two complexes approach to each other in a slipped, head-to-tail fashion with no or limited π-π stacking but where hydrogen bonds ensure supramolecular association.

## Conclusion

In this paper, we reported the Liquid Crystal behavior of 1) two purely organic compounds **1** and **2**, and 2) two new metal-omesogens, namely **Ru**<sub>1</sub> and **Ru**<sub>2</sub>. Combined experiments (Temperature dependent-SAXS,-FTIR, DSC, POM) and theoretical simulations allowed us to investigate in detail their supramolecular organization. Of outmost interest is the essential role of the hydrogen-bonding interactions, which literally drive and stabilize the supramolecular structures. Compound **1** and **2** behave as discotic mesogens, forming columnar arrangement with rectangular or oblique unit cell. Most striking is the change of packing mode accompanying the dimerization of **1** into **2**, going from head-to-tail to face-to-face. The introduction of the metal center along with its bulky coordination sphere induces some drastic modifications of the mode of organization, leading to a lamellar organization where the calamitic molecules arrange in rectangular or square lattices for **Ru**<sub>1</sub>. Such organization could be of interest for charge transport. Regarding **Ru**<sub>2</sub>, solid-state studies have clearly evidenced its liquid

crystal behavior but we failed obtaining any lattice parameters. Instead, we proposed a model packing based on observations of its behavior in solution (VT-NMR, FTIR, NOESY). This work contributes rationalizing the self-assembly of these calamitic and discotic molecules and opens new perspectives into the field of conductive metallomesogens for charge transport applications.

## Experimental Section

**General information.** Chemicals and solvents (HPLC, spectroscopic grade) were purchased from Merck-Sigma Aldrich, Acros Organics, Alfa Aesar, Fisher Scientific and were used without any further treatment. Anhydrous (HPLC) solvents were obtained from a MBraun SPS-800 drying system. Dry THF was obtained after distillation on Na/Benzophenone. Dry Diisopropylamine (DIPA), dry Triethylamine (TEA) and dry DMF were obtained after distillation on CaH<sub>2</sub> and kept in the dark on molecular sieves. All reactions were carried out under argon atmosphere using Schlenk techniques, unless otherwise stated. Schlenk tubes were dried under vacuum using heat-gun. TLC analyses were achieved on silica gel and bought from Fluka (silica gel matrix containing a fluorescent indicator at 254 nm). Column chromatography were performed on silica gel from Acros Organics (pore size of 60 Å, particle size of 40–63 μm) unless otherwise stated. <sup>1</sup>H, <sup>13</sup>C and <sup>31</sup>P-NMR spectra were recorded on a Bruker Avance III 400 MHz, Bruker AMX-3 300 (300 MHz) at 303 K. Relevant compounds were also characterized by 2D NMR using HSQC/HMQC, COSY <sup>1</sup>H-<sup>1</sup>H, HMBC sequences. VT-NMR were recorded on a Bruker 500 MHz Av III HD. Deuterated solvents were bought from Euriso-top. Solution sample and powder sample were acquired on FTIR Shimadzu IR affinity 1 or FTIR JASCO 4100. VT-FTIR spectra were acquired at the LASIRE facility (see supporting information for more details). HR-MS spectra were obtained from the Centre Régional de Mesures Physiques de l'Ouest (CRMPO). Differential scanning calorimetry (DSC) was carried out by using NETZSCH DSC 200 F3 instrument equipped with an intra-cooler. DSC traces were measured at 10 °C/min down to -25 °C. Optical microscopy investigations were performed on a Nikon H600 L polarizing microscope equipped with a Linkam "liquid crystal pro system" hotstage LTS420. Small-angle X-ray diffraction (SA-XRD) were performed using a Microstar Bruker rotating anode X-ray generator operated at 40 kV and 40 mA with monochromatic Cu Kα radiation (λ = 1.541 Å) and point collimation. The patterns were collected with a Mar345 Image-Plate detector (Marresearch, Norderstedt, Germany). The exposure time at each temperature was 3600 s and the heating or cooling speed between two temperatures was 10 °C/min. The samples were held in Lindeman glass capillaries (1.5 mm diameter). The capillaries were placed inside a Linkam HFX350-Capillary X-Ray stage which allow measurements from -196 °C up to 350 °C with an accuracy of 0.1 °C.

**Synthesis of **Ru**<sub>2</sub>.** A flame-dried Schlenk tube was charged with compound **1** (0.2 g, 0.13 mmol, 1 eq.) and [Ru(dppe)Cl]OTf (0.146 g, 0.13 mmol, 1.05 eq.) under argon flow. The tube was degassed thoroughly for 15–30 minutes then backfilled with argon. Dry DCM (16 mL) was added and the suspension was warmed at 35 °C to ensure solubility of the starting materials. At first dark-reddish, the mixture turned to brownish. The reaction was monitored by <sup>1</sup>H and <sup>31</sup>P{<sup>1</sup>H}-NMR and additional portions of the 16 electrons complex were necessary to drive the reaction to full consumption of **1**. The vinylidene intermediate was precipitated by adding dry Et<sub>2</sub>O (45 mL) and cannula-filtered. The solid was washed with dry Et<sub>2</sub>O (3x15 mL) and taken to dryness. The vinylidene intermediate was taken up in dry DCM (12 mL) and distilled Et<sub>3</sub>N (0.650 mL, 38 eq.) was added *via* a syringe. The solution instantaneously turned to

dark-yellow and was stirred at room temperature for c.a. 30 minutes. HPLC grade MeOH (40 mL) was then added to precipitate the target compound. After 15 minutes stirring at room temperature, the yellow solid was filtered-off, washed with MeOH (2x15 mL) and dried under vacuum to afford a yellow powder (0.250 g, 74% yield).  $^1\text{H}$  NMR (ppm, 300 MHz,  $\text{CD}_2\text{Cl}_2$ ) 7.72 (m, 4H,  $\text{H}_{\text{amide}} + \text{H}_{\text{Ar1}}$ ); 7.44–6.91 (m, 46H); 6.54 (d, 2H,  $^3J = 8.4$  Hz); 4.04 (m, 12H,  $\text{OCH}_2$ ); 2.71 (m, 8H,  $\text{CH}_{2,\text{dpppe}}$ ); 2.25 (s, 3H, Me); 1.89–1.70 (m, 12H,  $\text{H}_{\text{alk}}$ ); 1.28 (m, 112H,  $\text{H}_{\text{alk}}$ ); 0.88 (m, 18H,  $\text{CH}_{3,\text{alk}}$ ).  $^{13}\text{C}$  NMR (ppm, 100 MHz,  $\text{CD}_2\text{Cl}_2$ ) 166.2 (C=O), 153.8, 141.9, 137.2, 136.8, 136.5, 135.0, 134.4, 132.5, 132.5, 131.2, 131.0, 130.5, 129.8, 129.4, 129.2, 127.6, 127.4, 125.3, 122.39, 116.7, 114.7, 114.4, 112.1, 109.9, 106.2, 91.1, 89.0, 73.9, 69.83, 32.4, 31.0 (m,  $^1J_{\text{P,C}} + ^3J_{\text{P,C}} = 24$  Hz,  $\text{P}(\text{CH}_2)_2\text{P}$ ), 30.8, 20.2–29.8 (m), 26.6, 23.1, 14.3, 13.5.  $^{31}\text{P}\{^1\text{H}\}$  NMR (ppm, 162 MHz,  $\text{CD}_2\text{Cl}_2$ ) 49.4 (s). HRMS (ESI) 2491.3999 calculated for  $\text{C}_{155}\text{H}_{213}\text{N}_2\text{O}_8^{35}\text{ClP}_4^{102}\text{Ru}$  ( $\text{M}^+$ ): found 2491.4015. IR ( $\text{cm}^{-1}$ ): 3186 ( $\nu_{\text{N-H}}$ ), 3054 ( $\nu_{\text{C-H}}$ ), 2920 ( $\nu_{\text{C-H}}$ ), 2063 ( $\nu_{\text{C=C}}$ ), 1635 ( $\nu_{\text{C=O}}$ ), 1581 ( $\nu_{\text{C=C}}$ ).

## Acknowledgements

Part of this work has been performed using NMR spectrometer(s) belonging to the PRISM Multimodal Imaging and Spectroscopy Research Platform (Biogenouest©, UMS Biosit, Université de Rennes 1). Dr. De WAELE Isabelle thanks the Vibrational spectroscopy facility of the Advanced Characterization Platform of the Chevreul Institute. This work was granted access to the computing resources of CINES (Montpellier, allocations 2020-AP010811752, 2021-A0100805032 and 2021-AP0090811914 awarded by GENCI). Authors thank the Université de Rennes 1, the CNRS and the Agence Nationale de la Recherche (SAMAT, ANR-21-CE06-0012-01)

## Conflict of Interest

The authors declare no conflict of interest.

## Data Availability Statement

The data that support the findings of this study are available from the corresponding author upon reasonable request.

**Keywords:** Hydrogen bonds · Liquid crystals · Metallomesogens · Ru acetylides · Self-assembly

[1] a) Peter J. Collings, Michael Hird, *Introduction to Liquid Crystals: Chemistry and Physics*, CRC Press, 1997; b) D. Pauluth, K. Tarumi, *J. Mater.*

- Chem.* **2004**, *14*, 1219–1227; c) M. Schadt, *Annu. Rev. Mater. Sci.* **1997**, *27*, 305–379; d) C. Cuerva, M. Cano, C. Lodeiro *Chem. Rev.* **2021**, *121*, 12966–13010; e) J. W. Steed, J. L. Atwood, in *Supramolecular Chemistry 3rd edition*, Wiley-VCH, Weinheim, Germany 2022.
- [2] a) D. Pucci, B. Donnio, in *Handbook of Liquid Crystals*, Vol. 8 (Eds: J. W. Goodby, P. J. Collings, T. Kato, C. Tschierke, H. F. Gleeson, P. Raynes), Wiley-VCH, Weinheim, Germany 2014, Ch. 4; b) D. W. Bruce, R. Deschenaux, B. Donnio, D. Guillon, in *Metallomesogens. Comprehensive Organometallic Chemistry III*, Vol. 12, Elsevier 2007. Ch. 12.05.
- [3] K. Binnemans, *J. Mater. Chem. C* **2009**, *19*, 448–453.
- [4] a) T. Kato, M. Yoshio, T. Ichikawa, B. Soberats, H. Ohno, M. Funahashi, *Nat. Rev. Mater.* **2017**, *2*, 17001; b) T. Kato, M. Gupta, D. Yamaguchi, K. P. Gan, M. Nakayama, *Bull. Chem. Soc. Jpn.* **2021**, *94*, 357–376.
- [5] a) R. R. Parker, D. Liu, X. Yu, A. C. Whitwood, W. Zhu, J. A. Gareth Williams, Y. Wang, J. M. Lynam, D. W. Bruce, *J. Mater. Chem. C* **2021**, *9*, 1287–1302; b) T. C. Cooper, J. E. Haley, D. J. Stewart, S. Long, D. M. Krein, A. R. Burke, E. Arias, I. Moggio, G. Turlakov, R. F. Ziolo, M. Biler, M. Linares, P. Norman, *Adv. Funct. Mater.* **2020**, *309*, 1910562; c) Y. Kuroda, S. Nakamura, K. Srinivas, A. Sathyanarayana, G. Prabusankar, K. Hisano, O. Tsutsumi, *Crystals* **2019**, *9*, 227–240.
- [6] a) F. Camerel, R. Ziessel, B. Donnio, C. Bourgogne, D. Guillon, M. Schmutz, C. Lacovita, J. P. Bucher, *Angew. Chem. Int. Ed.* **2007**, *46*, 2659–2662; *Angew. Chem.* **2007**, *133*, 1–5; b) R. Ziessel, F. Camerel, B. Donnio, *Chem. Rec.* **2009**, *9*, 1–23.
- [7] M. J. Mayoral, P. Ovejero, J. A. Campo, J. V. Heras, E. Pinilla, M. R. Torres, C. Lodeiro, M. Cano *Dalton Trans.* **2008**, 6912–6924.
- [8] a) L. Norel, E. Di Piazza, M. Feng, A. Vacher, X. He, T. Roisnel, O. Maury, S. Rigaut, *Organometallics* **2014**, *33*, 4824–4835; b) H. Al Sabea, L. Norel, O. Galangau, H. Hijazi, R. Metivier, T. Roisnel, O. Maury, C. Bucher, F. Riobe, S. Rigaut, *J. Am. Chem. Soc.* **2019**, *141*, 20026–20030.
- [9] O. Galangau, D. Daou, N. El Beyrouiti, E. Caytan, C. Meriadec, F. Artzner, S. Rigaut, *Inorg. Chem.* **2021**, *60*, 11474–11484.
- [10] A. Mulas, Y. M. Hervault, X. He, E. Di Piazza, L. Norel, S. Rigaut, C. Lagrost, *Langmuir* **2015**, *31*, 7138–7147.
- [11] H. K. Bisoyi, Q. Li, *Chem. Rev.* **2016**, *116*, 15089–15166.
- [12] a) R. Ziessel, G. Pickaert, F. Camerel, B. Donnio, D. Guillon, M. Cesario, T. Prange, *J. Am. Chem. Soc.* **2004**, *126*, 12403–12413; b) F. Camerel, L. Bonardi, G. Ulrich, L. Charbonnière, B. Donnio, C. Bourgogne, D. Guillon, P. Retailleau, R. Ziessel, *Chem. Mater.* **2006**, *18*, 5009–5021; c) F. Camerel, B. Donnio, C. Bourgogne, M. Schmutz, D. Guillon, P. Davidson, R. Ziessel, *Chem. Eur. J.* **2006**, *12*, 4261–4274.
- [13] S. Laschat, A. Baro, N. Steinke, F. Giesselmann, C. Haegele, G. Scalia, R. Judele, E. Kapatsina, S. Sauer, A. Schreivogel, M. Tosoni, *Angew. Chem. Int. Ed.* **2007**, *46*, 4832–4887.
- [14] a) M. Hartlieb, E. D. H. Mansfield, S. Perrier, *Polym. Chem.* **2020**, *11*, 1083–1110; b) K. Tambara, J.-C. Olsen, D. E. Hansen, G. D. Pantoş, *Org. Biomol. Chem.* **2014**, *12*, 607–614; c) R. B. Martin, *Chem. Rev.* **1996**, *96*, 3043–3064; d) T. F. A. de Greef, E. W. Meijer, *Nature* **2008**, *453*, 171; e) T. F. A. de Greef, M. M. J. Smulders, M. Wolffs, A. P. H. J. Schenning, R. P. Sibesma, E. W. Meijer, *Chem. Rev.* **2009**, *109*, 5687–5754.
- [15] a) D. Zhao, J. S. Moore, *Org. Biomol. Chem.* **2003**, *1*, 3471–3491; b) M. M. J. Smulders, M. M. L. Nieuwenhuizen, T. F. A. de Greef, P. van der Schoot, A. P. H. J. Schenning, E. W. Meijer, *Chem. Eur. J.* **2010**, *16*, 362–367; c) H. M. M. ten Eikelder, A. J. Markvoort, T. F. A. de Greef, P. A. J. Hilbers, *J. Phys. Chem. B* **2012**, *116*, 5291–5301.

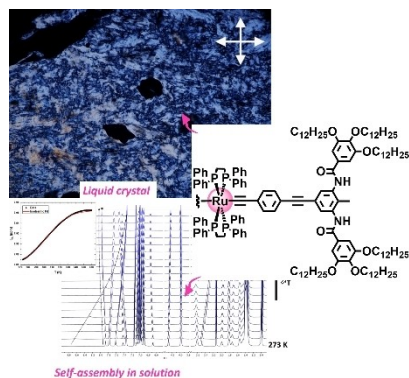
Manuscript received: September 9, 2022

Revised manuscript received: October 12, 2022

Accepted manuscript online: October 13, 2022

# RESEARCH ARTICLE

In the present article, we report the liquid crystal and self-assembly abilities of new Ru<sup>II</sup> acetylide complexes and their organic counterparts. The four compounds show mesogenic properties. Importantly, introducing the metal center and its bulky coordination sphere dramatically changes the supramolecular packing at the solid state. When the metal bears only one acetylide ligand, self-assembly occurs in the solution state, yet with no solvent gelation.



Dr. O. Galangau\*, Dr. E. Caytan, W. T. Gallonde, Dr. I. de Waele, Dr. F. Camerel\*, Prof. S. Rigaut\*

1 – 10

**Solid-State and Solution Self-assembly Properties of Mono- and Bis-acetylide Ru<sup>II</sup> Complexes Bearing Hydrogen-Bonding Amide Functions**

